molecular pharmaceutics

Article

pubs.acs.org/molecularpharmaceutics

Formulation of Anti-miR-21 and 4-Hydroxytamoxifen Co-loaded Biodegradable Polymer Nanoparticles and Their Antiproliferative Effect on Breast Cancer Cells

Rammohan Devulapally, Thillai V. Sekar, and Ramasamy Paulmurugan*

Molecular Imaging Program at Stanford, Bio-X Program, Canary Center at Stanford for Cancer Early Detection, Department of Radiology, Stanford University School of Medicine, Stanford University, 3155 Porter Drive, Palo Alto, California 94304, United States

Supporting Information

ABSTRACT: Breast cancer is the second leading cause of cancer-related death in women. The majority of breast tumors are estrogen receptor-positive (ER+) and hormone-dependent. Neoadjuvant anti-estrogen therapy has been widely employed to reduce tumor mass prior to surgery. Tamoxifen is a broadly used anti-estrogen for early and advanced ER+ breast cancers in women and the most common hormone treatment for male breast cancer. 4-Hydroxytamoxifen (4-OHT) is an active metabolite of tamoxifen that functions as an estrogen receptor antagonist and displays higher affinity for estrogen receptors than that of tamoxifen and its other metabolites. MicroRNA-21 (miR-21) is a small noncoding RNA of 23 nucleotides that regulates several apoptotic and tumor suppressor genes and contributes to chemoresistance in numerous cancers, including breast cancer. The present study investigated the therapeutic potential of 4-OHT and anti-miR-21 coadministration in an attempt to combat tamoxifen resistance, a common problem often encountered in anti-estrogen therapy. A biodegradable poly(D,L-lactide-*co*-glycolide)-*block*-poly(ethylene glycol) (PLGA-*b*-PEG-COOH) copolymer was utilized as a carrier to codeliver 4-OHT and anti-miR-21 to ER+ breast cancer cells. 4-OHT and anti-miR-21 co-loaded PLGA-*b*-PEG nanoparticles (NPs) were developed using emulsion-diffusion evaporation (EDE) and water-in-oil-in-water (w/o/w) double emulsion methods. The EDE method was found to be best method for 4-OHT loading, and the w/o/w method proved to be more effective for coloading NPs with anti-miR-21 and 4-OHT. The optimal NPs, which were prepared using the double emulsion method, were evaluated for their antiproliferative and apoptotic effects against MCF7, ZR-75-1, and BT-474 human breast cancer cells as well as against 4T1 mouse mammary carcinoma cells. We demonstrated that PLGA-*b*-PEG NP encapsulation significantly extended 4-OHT's stability and biological activity compared to that of free 4-OHT. MTT assays indicated that treatment of MCF7 cells with 4-OHT−anti-miR-21 co-loaded NPs resulted in dose-dependent antiproliferative effects at 24 h, which was significantly higher than what was achieved with free 4-OHT at 48 and 72 h post-treatment. Cell proliferation analysis showed that 4-OHT and anti-miR-21 co-loaded NPs significantly inhibited MCF-7 cell growth compared to that of free 4-OHT (1.9-fold) and untreated cells (5.4-fold) at 1 μM concentration. The growth rate of MCF7 cells treated with control NPs or NPs loaded with anti-miR-21 showed no significant difference from that of untreated cells. These findings demonstrate the utility of the PLGA-*b*-PEG polymer NPs as an effective nanocarrier for co-delivery of anti-miR-21 and 4-OHT as well as the potential of this drug combination for use in the treatment of ER+ breast cancer.

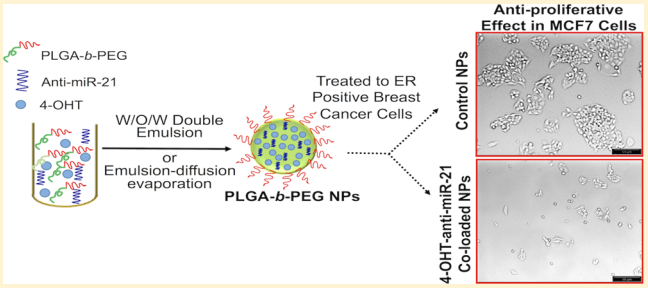

KEYWORDS: *polymer nanoparticles, PLGA, 4-hydroxytamoxifen (4-OHT), microRNA-21, anti-miR's, estrogen receptor, breast cancer therapy*

INTRODUCTION

Breast cancer is the most common malignancy and a leading cause of cancer-related death in women worldwide.[1] The single-therapeutic approach using traditional chemotherapy often fails to succeed largely due to multidrug resistance (MDR) in cancer cells. MDR is thus a major obstacle in effective cancer chemotherapy. There is evidence to suggest that the coadministration of small interfering RNAs (siRNAs), anticancer drugs, and anticancer MDR-reversing agents has the potential to improve cancer treatment success rates[2−6] and the efficacy of chemotherapy.[7] However, most anticancer drugs and anticancer MDR-reversing agents have very limited therapeutic potential due to high inherent toxicities.[8] Consequently, despite their potential utility, further chemotherapeutic development and advancements in targeted delivery systems are required before

Received: December 20, 2014
Revised: March 26, 2015
Accepted: April 16, 2015
Published: April 16, 2015

DOI: 10.1021/mp500852s
Mol. Pharmaceutics 2015, 12, 2080−2092

they can be employed in cancer therapy. Moreover, despite the improvement in current cancer therapeutics, enhancements in chemotherapeutics and targeted delivery systems are much needed for effective cancer therapy.[9]

4-Hydroxytamoxifen (4-OHT) is a selective estrogen receptor modulator (SERM). It is an active metabolite of pro-drug tamoxifen (TAM), which acts as an estrogen receptor antagonist.[10,11] TAM and 4-OHT are cytostatic drugs. They do not induce any cytotoxicity in cells, but they inhibit estradiol-induced cell proliferation by competitively binding to estrogen receptor. Normally, this process will not affect nonproliferating normal cells. In contrast, breast tissues undergo substantial programmed cell proliferation and apoptosis during every menstrual cycle. During this time, various glandular and epithelial cells will be in proliferative status. Hence, TAM treatment can have a cytostatic effect on these normal proliferating cells. Neoadjuvant anti-estrogen therapy using TAM has been widely used to treat estrogen receptor positive (ER+) breast cancer patients.[9,12,13] 4-OHT has a greater binding affinity to estrogen receptors than TAM and has a ∼100−167-fold higher potency in inhibiting cell proliferation in both breast cancer cells[14−16] and normal human breast cells.[17] Anti-estrogenic 4-OHT has both *Z* (*trans*) and *E* (*cis*) isomeric forms. It has been reported that the *trans* isomer of 4-OHT has a 100-fold higher anti-estrogenic potency than the *cis* isomer in ER+ T47D breast cancer cells[18,19]

4-OHT and its pro-drug TAM have been prescribed to patients before surgery in order to reduce breast tumor mass and have been shown to lower the risk of the local tumor recurrence by inhibiting induction of new primary tumors.[20−24] However, 4-OHT is practically insoluble in water and is soluble in ethanol and methanol. 4-OHT displays poor oral bioavailability when administered as free drug, and it is associated with various adverse effects, including nausea, hot flushes, and weight gain. Effective delivery systems that enable slow-release strategies while protecting drug stability may improve the bioavailability of 4-OHT and simultaneously avoid its adverse side effects. However, while there has been an interest in developing biodegradable polymer nanoparticles (NPs) for neoadjuvant 4-OHT delivery,[9] limited reductions in breast tumor mass have been achieved with 4-OHT monotherapy.

MicroRNAs are endogenously expressed noncoding small RNA molecules that regulate cellular pathways by controlling the expression of various genes. MicroRNA-21 (miR-21) is a key microRNA that is overexpressed in most human cancers, including breast cancer, and has been shown to contribute to tumor growth, metastasis, and MDR.[25,26] In the analysis of 157 human miRs, only miR-21 was consistently overexpressed in breast tumors in comparison to matched normal breast tissues.[25] The antisense oligonucleotide 100% complementary to miR-21 (anti-miR-21) has been reported to inhibit migration and invasion of cancer cells by blocking the function of endogenous miR-21 while enhancing the cancer cell's response to chemotherapeutic agents.[27,28] Overexpression of miR-21 is linked with the development of MDR in breast cancer; hence, targeting miR-21 is a unique and aspiring MDR-reversing approach in cancer therapy.[2] Transfection of antisense-miR-21 in MCF7 cells has been shown to suppress tumor cell growth *in vitro* (in culture) and *in vivo* (tumor xenograft in a mouse model).[25] However, despite the development of structurally modified miRs, delivery of naked miRs to tumor cells *in vivo* remains a challenge owing to their degradation by serum nucleases, poor cellular uptake, and off-target effects.[29,30]

While numerous delivery platforms have been reported for TAM delivery,[9,31] and a few nanoparticle formulations have been reported for the delivery of 4-OHT[32−36] and anti-miR-21,[2,37,38] there is no formulation reported for the co-delivery of TAM or 4-OHT and anti-miR-21. Co-delivery of anti-miR-21 and 5-fluorouracil (5-FU), through poly(amidoamine) dendrimer NPs, substantially improved the cytotoxicity of 5-FU, strongly enhanced the apoptosis of U251 glioma brain tumor cells, and significantly diminished the migration ability of the tumor cells.[37] This study also indicates that simultaneous co-delivery of anti-miR-21 and 5-FU might have substantial applications in the treatment of miR-21-overexpressing glioblastomas. Anti-miR-21-loaded and chlorotoxin-coupled liposomal NPs significantly reduced the growth of U87 human glioblastoma multiforme cell lines.[38] Anti-miR-21 and adriamycin (ADR) co-loaded multifunctional polymer nanocomplexes substantially improved the accumulation of ADR in ADR-resistant MCF7 cells.[2] This resulted in much higher cytotoxicity than what was observed in cells treated with free ADR, indicating that this polymer nanocomplex might effectually reverse ADR resistance in MCF7 cells. In another study,[33] 4-OHT-loaded pH-gradient pegylated liposomes were formulated by varying the composition of lipids and external pH for 4-OHT loading and were delivered to MCF7 cells as well as in multiple myeloma (MM) cells.[32,33] These liposomes resulted in greater stability, low relative toxicity, and slow 4-OHT release compared to that of conventional non-pH-gradient liposomes, and they blocked MM tumor growth at 4 mg/kg/week *in vivo* after 6 weeks of treatment. These findings were supported by another investigation that showed that 4-OHT-nanodiamond complexes significantly reduced MCF7 cell viability compared to the negative control *in vitro*.[36]

Poly(lactic-*co*-glycolic acid) (PLGA) is a well-established biodegradable and biocompatible polymer whose hydrolysis releases glycolic acid and lactic acid monomers, which are easily metabolized by the body without any side effects.[9] Poly(ethylene glycol) (PEG) is another well-recognized, biocompatible, and nonhazardous polymer. While hydrophobic PLGA has been shown to entrap the drugs, the hydrophilic PEG is known to shield NPs from the immune surveillance and improve the enhanced permeability and retention (EPR) effect.[9] Biodegradable PLGA-PEG block copolymer NPs have thus attracted great interest for various drug delivery approaches.[9,39−44] Anti-miR-21 and anti-miR-10b co-loaded urokinase plasminogen activator receptor targeted PLGA-*b*-PEG NP-treated mice showed significant reduction in triple-negative breast cancer tumor growth compared to the control NP-treated mice in *in vivo* tumor xenografts.[41] These PLGA-*b*-PEG NPs, when combined with microbubbles, delivered 7.2-fold higher miR-122 into tumors with ultrasound compared to that from treatment without ultrasound.[42]

We hypothesize that co-delivery of anti-miR-21 and 4-OHT could concurrently affect target miR-21 and ER receptor signaling, which would results in an enhanced therapeutic effect. Herein, we report the optimal synthesis of biodegradable polymer nanoparticles from poly(D,L-lactide-*co*-glycolide)-*block*-poly(ethylene glycol) (PLGA-*b*-PEG-COOH) as a carrier for the co-delivery of anti-miR-21 and 4-OHT as well as the evaluation of the carrier's significant antiproliferative effects in ER+ MCF7, ZR-75-1, and BT-474 human breast cancer cells and 4T1 mouse mammary carcinoma cells *in vitro*.

DOI: 10.1021/mp500852s
Mol. Pharmaceutics 2015, 12, 2080−2092

EXPERIMENTAL SECTION

Materials. All chemical used in this study were of analytical grade or above and purchased from commercial suppliers. 4-Hydroxytamoxifen (≥70% *Z* isomer) ≥98%, carboxy-terminated poly(D,L-lactide-*co*-glycolide) (PLGA, MW 7000−17000, inherent viscosity 0.16−0.24 dL/g), *N*-hydroxysuccinimide (NHS) 98%, and *N*-(3-(dimethylamino)propyl)-*N*′-ethylcarbodiimide hydrochloride (EDC) ≥99.0% were obtained from Sigma-Aldrich (St. Louis, MO, USA). Heterobifunctional PEG polymer (NH_2-PEG-COOH, MW 3400) was purchased from JenKem Technology (Allen, TX, USA) and NOF Corporation (Irvine, CA, USA). Anti-miR-21-PS were custom-synthesized by the PAN facility at Stanford at a purity > 95%. Cell culture media, charcoal-stripped fetal bovine serum (FBS), and streptomycin and penicillin (PS) were purchased from Invitrogen (Carlsbad, CA, USA). MCF7, ZR-75-1, BT-474, and 4T1 breast cancer cell lines were purchased from American Type Culture Collection (ATCC) (Manassas, VA, USA). After receiving cell lines from the supplier, they were grown, subcultured, frozen, and stored under liquid nitrogen vapor for future use. All experiments in this article were done before cells reached 40 passages.

Synthesis of PLGA-*b*-PEG-COOH Copolymer. PLGA-COOH (0.04166 mmol, 500 mg) was dissolved in dry dichloromethane (CH_2Cl_2). To this was added EDC (0.4166, 80 mg) in dry CH_2Cl_2 and subsequently NHS (0.4166 mmol, 48 mg) in dry CH_2Cl_2, and the mixture was stirred at room temperature (RT) for 4 h. The resulted PLGA-NHS was precipitated using cold methanol (MeOH)/diethyl ether (Et_2O) (1:1). The precipitate was centrifuged at 5000 rpm for 5 min, the supernatant was decanted, and the pellet was further washed twice with cold MeOH/Et_2O (1:1). The pellet was dried under vacuum for 3 h. The dried PLGA-NHS pellet (0.04132 mmol, 500 mg) was dissolved in dry chloroform and treated with heterobifunctional NH_2-PEG-COOH (0.04132 mmol, 140 mg) followed by addition of diisopropylethyamine (0.4132 mmol, 72 μL). The reaction mixture was stirred at RT for 24 h. The resulted PLGA-*b*-PEG-COOH was precipitated by addition of cold MeOH/Et_2O (1:1), washed twice with cold MeOH/Et_2O (1:1), dried under vacuum, and characterized by ^{1}H NMR (yield: 74%).

Formulation and Characterization of 4-Hydroxytamoxifen, Anti-miR-21 Co-loaded PLGA-*b*-PEG-NPs by Emulsion-Diffusion Evaporation (EDE). A premixed solution of 4-OHT and PLGA-*b*-PEG-COOH (10 mg) in ethyl acetate was added dropwise to the 2% poly(vinyl alcohol) (PVA) (w/v) with mild stirring. The resulted mixture was sonicated at 60% amplitude for 1 min at 0 °C using a sonic dismembrator to produce the primary emulsion. The primary emulsion was diffused by addition of ultrapure water and stirred at RT for 3 h to evaporate the ethyl acetate and harden the NPs. The resulted NPs were sterile filtered using 0.45 μM syringe filter and washed using centrifugal filters (100 kDaA MWCO, EMD-Millipore, USA) to remove nonencapsulated 4-OHT. The concentrated NPs were further washed with DNase/RNase-free water three times. The nanoparticles were diluted to a known volume and lyophilized with 10% sucrose, and the resulted NPs powder was stored at −20 °C. NPs containing anti-miR-21 individually and co-loaded with 4-OHT were prepared by addition of anti-miR-21/spermidine complex to 2% PVA solution. The prepared NPs size was estimated by dynamic light scattering (DLS), TEM, and loaded 4-OHT and anti-miR-21 concentrations.

Formulation and Characterization of 4-Hydroxytamoxifen, Anti-miR-21 Co-loaded PLGA-*b*-PEG-NPs by Water-in-Oil-in-Water Double Emulsion (w/o/w) Method. The 4-hydroxytamoxifen and anti-miR-21-PS, Cy5−anti-miR-21-PS co-loaded PLGA-PEG block copolymer NPs were formulated using a modified water-in-oil-in-water double emulsion solvent evaporation method.[45] Anti-miR-21 (9 nmol) and cy5−anti-mR-21 (1 nmol) were complexed with spermidine in a N/P ratio of 15:1 at room temperature for 15 min in DNase/RNAase-free water. This anti-miR-21−spermidine complex solution was added dropwise to the premixed solution of 4-OHT and PLGA-*b*-PEG-COOH (10 mg) in CH_2Cl_2 with mild stirring. The resulted mixture was sonicated at 40% amplitude for 1 min at 0 °C using a sonic dismembrator to produce the primary emulsion. 1% Poly(vinyl alcohol) (PVA) (w/v) in DNase/RNase-free water was added to the primary emulsion, and the mixture was sonicated at 40% amplitude for 1 min at 0 °C and stirred at RT for 3 h to evaporate the CH_2Cl_2 and harden the NPs. The resulted NPs were centrifuged using sterile centrifugal filters (100 kDaA MWCO, EMD-Millipore, USA), and the concentrated NPs were washed with DNase/RNase-free water three times. The nanoparticles were diluted to a known volume and lyophilized with 10% sucrose, and the resulted NPs powder was stored at −20 °C. The NPs size was estimated by dynamic light scattering (DLS), TEM, loaded 4-OHT and anti-miR-21 concentrations, and *in vitro* studies. The plain control PLGA-*b*-PEG NPs and 4-OHT individually loaded PLGA-*b*-PEG NPs were also prepared using a similar procedure by eliminating the anti-miR-21/spermidine step.

Particle Size and Zeta-Potential Measurements. Particle size and zeta potential values of NPs were performed using a Zetasizer-90 (Malvern Instruments, UK). Size measurement was performed at 25 °C at a 90° scattering angle. The mean hydrodynamic diameter was determined by the cumulant method. Zeta-potential measurements were made using the Smoluchowski model and using an aqueous dip cell in automatic mode.

Entrapment Efficiency Estimation for Anti-miR-21. To calculate the entrapment efficiency of anti-miR-21, the anti-miR-21 from NPs and wash solution were concentrated by freeze drying at −80 °C and resuspended in a known volume of DNase/RNase-free water. The standard anti-miR-21 (10% Cy5) and ant-miR-21 extracted from NPs and wash solution were electrophoresed in a 3% agarose gel at 80 V for 20 min and imaged by a UV-Chemdoc. Imaging the fluorescence of co-encapsulated Cy5−anti-miR-21 was performed using an optical CCD camera with excitation at 570 nm and with a Cy5 emission filter (IVIS Lumina, Caliper). The acquired chemdoc images were quantified by densitometry, and the fluorescence images by IVIS Living Image quantitation software after drawing the ROI.

The entrapment efficiency from the NPs was calculated using following formula

$$\text{entrapment efficiency (\%)} = \text{mass of total anti-miR-21 found in freeze-dried NPs (W)} / \text{mass of total anti-miR-21 used (M)} \times 100$$

The entrapment efficiency based on wash solution was calculated using following formula

$$\text{entrapment efficiency (\%)} = \text{mass of total anti-miR-21 used (M)} - \text{mass of free anti-miR-21 in the wash solution (W)}/\text{M} \times 100$$

DOI: 10.1021/mp500852s
Mol. Pharmaceutics 2015, 12, 2080−2092

Entrapment Efficiency Estimation for 4-OHT. Entrapment efficiency was calculated by high-performance liquid chromatography (HPLC) using a C18 column and acetonitrile−water mobile phase. The entrapment efficiency of 4-OHT from the NPs was calculated using following formula.

$$\text{entrapment efficiency (\%)} = \text{mass of total 4-OHT found in freeze-dried NPs (W)} / \text{mass of total 4-OHT used (M)} \times 100$$

Transmission Electron Microscopy (TEM). Transmission electron microscopy images were obtained using a FEI TITAN 80-300kV ETEM (environmental transmission electron microscope) at Stanford's Nanocharacterization Laboratory by operating at 80 kV using negative-stained NPs. In brief, for negative staining, a drop (~5 μL) of PLGA-*b*-PEG NPs was mixed with a drop of 1% phosphotungstic acid (PTA) (the pH of PTA was adjusted to 7.5 with 1 N NaOH), and the solution was incubated for 3 min. Then, a drop of PTA-stained NPs was plated on a carbon film-coated copper grid and allowed to sit for 3 min, excess solution was drained off, and the sample was air-dried and observed under TEM. Size analysis was done using ImageJ software.

Dose Study Analysis by MTT Assay. 4-OHT−anti-miR-21 NPs' dose and cell viability were assessed by MTT assay according to the manufacturer's protocol (Invitrogen, USA). Briefly, MCF7 (1.56×10^4 cells/cm^2 or 5000 cells/well) were seeded in 96-well tissue culture plates and incubated for 24 h. After 24 h, cells were incubated with free 4-OHT and 4-OHT−anti-miR-21 NPs at various concentrations for 24−72 h at 37 °C and 5% CO_2 in phenol-red-free RPMI growth medium supplemented with 2% charcoal-treated FBS. Untreated cells were used as a negative control. After each time point, the media was carefully removed and the cells were carefully washed with PBS. Cells were then replenished with 90 μL of phenol-red-free media with 10 μL of MTT stock (12 mM) solution and incubated for 3 h; then, media was aspirated carefully without disturbing the precipitate, 50 μL of DMSO was added, and the precipitate was kept at 37 °C for 20 min to dissolve the metabolically reduced tetrazolium MTT precipitate from the cells. Absorbance of supernatant was measured at 540 nm using a multiwell plate reader (Infinite 2100, Tecan, Männedorf, Switzerland). For each set of conditions, the experiments were performed in triplicate. The relative cell viability (%) compared to control cells was calculated as follows: cell viability (%) = [Abs (sample) − Abs (blank)/Abs (control) − Abs (blank)] × 100.

Cell Proliferation Assay. To examine the cell proliferation of MCF7, ZR-75-1, BT-474, and 4T1 (1.05×10^4 cells/cm^2 or 100 000 cells/well, triplicate), cells were seeded in 6-well tissue culture plates and incubated for 24 h with phenol-red-free RPMI medium (supplemented with 2% charcoal-stripped FBS, 1% penicillin−streptomycin) at 37 °C and 5% CO_2. The cells were then treated with free 4-OHT or 4-OHT and anti-miR-21 co-loaded NPs at their respective concentrations. After 24 h, cells were washed with PBS and further incubated with 2% phenol-red-free RPMI medium for 5 days. The cells were tested for the presence of fluorescence signals under an inverted fluorescent microscope. After 5 days of incubation, cells were trypsinized, and the collected cells were used for flow cytometry, immunoblotting analysis, and counting on a hemocytometer (triplicate) to analyze proliferation.

Flow Cytometry for PI-Based Apoptosis Analysis. For flow cytometry analysis, after incubation with different NPs, MCF7 cells were trypsinized and washed, and all of the washed and trypsinized cells were combined and analyzed for dead or apoptotic cells by staining with propidium iodide (15 nM) for 15 min followed by flow cytometry (FACS Aria III, BD Biosciences, San Jose, CA, USA) at the Stanford FACS Facility. Data were analyzed by FlowJo FACS analysis software (Tree Star, Ashland, OR, USA). GCV and CB1954 were purchased from Sigma-Aldrich (St. Louis, MO, USA).

Immunoblot Analysis. For immunoblot analysis, after incubation with different NPs, MCF7 and ZR-75-1 cells were trypsinized and washed, and the collected cell pellets were lysed in RIPA buffer supplemented with protease inhibitor cocktail (Pierce Biotechnology, Rockford, IL, USA). The lysates were sonicated thoroughly to ensure complete lysis of the cells. Lysates were then centrifuged at 16 000 g at 4 °C for 15 min, and the supernatant was collected. Protein content of the each supernatant solution was estimated by Bradford assay kit (Bio-Rad) and normalized. Normalized proteins (15 μL) were incubated with the mixture of SDS loading dye/2-mercaptoethanol (5 μL, 10:1) at 100 °C for 5 min, resolved by 4−12% gradient SDS/PAGE (Invitrogen), and electroblotted onto a nitrocellulose membrane (0.45 μM pore size, Schleicher & Schuell). Prestained protein marker (New England Biolabs, Ipswich, MA) was used at every run to confirm the molecular mass and complete transfer of protein to the membrane. The membrane was washed three times (5 min each) with TBS-T buffer. The membrane was blocked in 10% of nonfat dry milk in TBS-T buffer for 1 h. The membrane was further incubated in the same blocking solution with respective antibody (1:1000) overnight at 4 °C on a rotating platform. The membrane was washed with TBS-T buffer three times and incubated with HRP-conjugated anti-rabbit antibody (1:4000) in TBS-T buffer for 1 h at room temperature. The membrane was washed three times with TBS-T buffer before incubation with the chemiluminescent HRP substrate LuminoGlo (Cell Signaling, Beverly, MA), and the membrane was imaged with an IVIS Lumina imaging system (Caliper Life Sciences, Alameda, CA). Images were analyzed by IVIS Living Image software. The same membrane was stripped and reprobed with another antibody and finally with GAPDH to control for protein loading.

Intracellular Release and Stability of PLGA-*b*-PEG-NP Loaded Anti-miR-21 in Cells by qRT-PCR Analysis. To examine the stability and relative level of anti-miR-21, MCF7 (1.05×10^4 cells/cm^2 or 100 000 cells/well in triplicate) cells were seeded in seven 6-well tissue culture plates and incubated for 24 h with phenol-red-free RPMI medium (supplemented with 2% charcoal-treated FBS, 1% penicillin−streptomycin) at 37 °C and 5% CO_2. The cells were then treated with anti-miR-21 and 4-OHT co-loaded NPs. After 24 h, the first plate of cells was washed with PBS and immediately flash frozen and stored at −80 °C until completion of all time points. The treated cells in the second to sixth plates were frozen and stored similarly after the completion of the treatment time. After collecting samples from all of the time points, the cells were lysed with RNA binding buffer, and miRNA was extracted using an Ambion RNA extraction kit according to the manufacturer's protocol (Life Technologies, USA). The isolated RNA was quantified using a Qubit RNA assay kit according to the manufacturer's protocol (Life Technologies, USA). Quantified RNAs (15 ng each) were used for the analysis of anti-miR-21 level by quantitative real-time

DOI: 10.1021/mp500852s
Mol. Pharmaceutics 2015, 12, 2080−2092

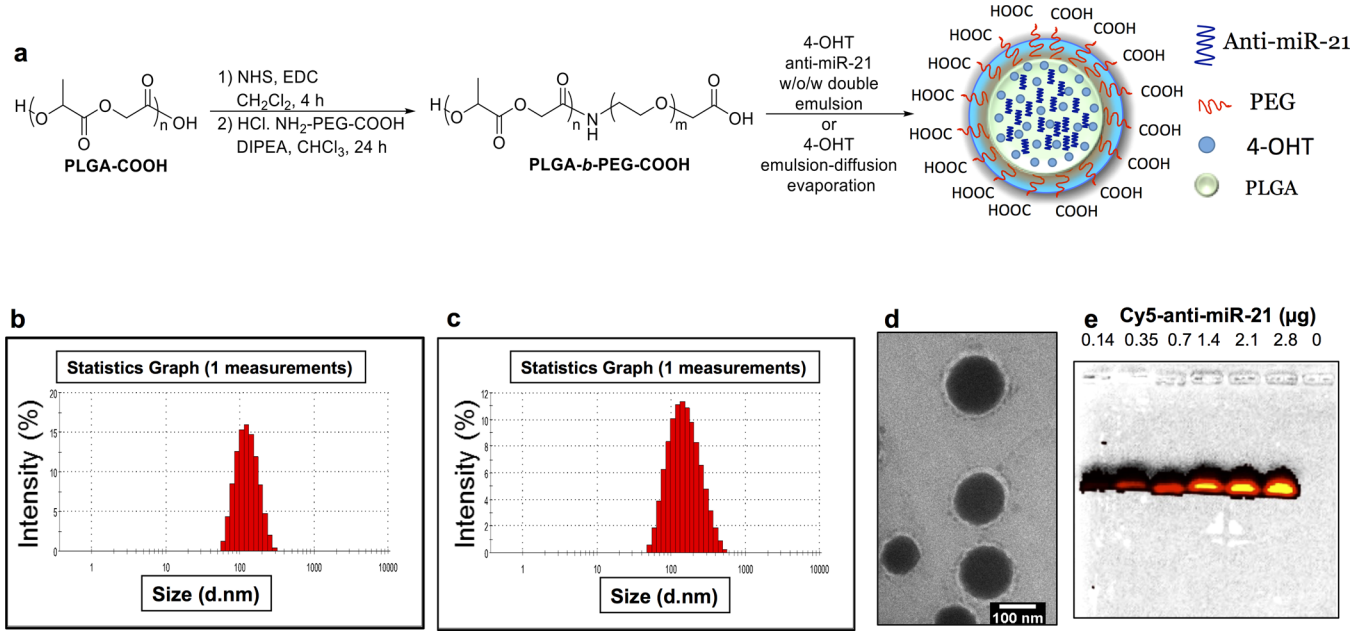

Figure 1. (a) Synthesis and formulation of PLGA-*b*-PEG NPs. (b) Hydrodynamic particle size measurement of NPs prepared by EDE by dynamic light scattering (DLS). (c) DLS of NPs prepared by the w/o/w double emulsion method. (d) TEM images of PLGA-*b*-PEG NPs prepared by w/o/w double emulsion method. (e) Estimation of anti-miR-21 loading in PLGA NPs by imaging the co-loaded Cy5−anti-miR-21 using an IVIS spectrum optical CCD camera with excitation at 570 and a Cy5 emission filter after resolving the samples by 3% agarose gel electrophoresis.

RT-PCR using a custom designed TaqMan probe according to the manufacturer's protocol (Life Technologies, USA).

4-OHT Stability Analyses by Reporter Protein Complementation Assay Using Genetically Engineered SkBr3 Cells Constitutively Expressing NFluc−ER-LBD−CFluc Fusion Protein. SkBr3 cells stably expressing an NFluc−ER-LBD−CFluc fusion protein (5000 cells/well) were seeded in 96-well tissue culture plates and incubated for 24 h. After 24 h, cells were incubated with free 4-OHT or 4-OHT−anti-miR-21 co-loaded NPs at various concentrations for 24−72 h at 37 °C and 5% CO_2 in DMEM growth medium supplemented with 10% charcoal-stripped FBS and 1% penicillin−streptomycin. Untreated cells were used as a negative control. One plate was used for the reporter protein complementation assay, and another plate, for an MTT assay. After each time point, the media was carefully removed, and cells were then replenished with 50 μL of 30 μg/mL D-luciferin solution in PBS and imaged for bioluminescence signal using an IVIS Lumina imaging system (Caliper Life Sciences, MA) for 25 min with an integration time of 1 min each. The image with the peak signal was used for data analysis. The other plate was used for MTT assay analysis. Data was analyzed by dividing the peak signal from the IVIS Lumina imaging system and MTT assay values for the reporter protein complementation assay.

Statistical Analysis. The statistical significance of the studies was analyzed using Student's *t* test. Differences with *p* values of less than 0.05 were considered to be significant.

RESULTS AND DISCUSSION

Nanoparticle Preparation and Characterization. PLGA-*b*-PEG copolymer was synthesized from the conjugation of acid-terminated PLGA-COOH and heterobifunctional amino-PEG-carboxylic acid (H_2N-PEG-CO_2H) (Figure 1a).[46] Since 4-OHT is practically water-insoluble, we formulated PLGA-*b*-PEG NPs loaded with 4-OHT by using an emulsion-diffusion evaporation (EDE) method with poly(vinyl alcohol) (PVA) as an emulsifier

Table 1. NPs Size Using Various Organic Solvents at Different Sonication Times by Emulsion-Diffusion Evaporation (EDE)

entry	sonication time (min) at 60% amplitude	organic solvent[a]	Size (nm)[b,c]
1	1	ethyl acetate	115.7 ± 2.15
2	2	ethyl acetate	108.0 ± 1.60
3	4	ethyl acetate	104.1 ± 1.60
4	15	ethyl acetate	101.1 ± 1.77
5	1	dichloromethane	123.4 ± 2.32
6	5	DMF	112.3 ± 3.20

[a]2% PVA in aqueous solution used for emulsification. [b]Average of three DLS measurements. [c]After sonication, NPs were stirred for 3 h to allow for organic solvent evaporation and hardening of the NPs.

to stabilize the NPs. However, we recognized that a single emulsion may not be suitable for loading highly hydrophilic anti-miR-21. Subsequently, we optimized the formulation for co-loading both 4-OHT and anti-miR-21 (10% Cy5−anti-miR-21 + 90% anti-miR-21) by employing the water-in-oil-in-water (w/o/w) double emulsion method, again using PVA to stabilize NPs (Figure 1a). We compared both EDE and the water-in-oil-in-water double emulsion method for co-loading both 4-OHT and anti-miR-21. Cy5-conjugated anti-miR-21 (10%) was used for visualizing the delivery of the NPs into the cells through fluorescent microscopy. Dynamic light scattering (DLS) of the NPs, which were prepared by both methods, showed size ranges of 100−200 nm (Figure 1b,c) with a polydispersity index (PDI) of 0.08−0.21 and a surface charge in the range of −14 to −22 mV. The morphology and size of NPs were further confirmed by transmission electron microscopy (Figure 1d). The entrapment efficiency of 4-OHT from synthesized NPs was calculated using high-performance liquid chromatography (HPLC). Anti-miR-21 loading was calculated using a Quant-iT RNA assay kit, and optical CCD camera imaging-based quantification for the co-loaded Cy5−anti-miR-21 was performed after resolving the samples in a 3% agarose gel (Figure 1e).

DOI: 10.1021/mp500852s
Mol. Pharmaceutics 2015, 12, 2080−2092

Table 2. Size, 4-OHT and Anti-miR-21 Loading Percentage, and Number of Anti-miR-21 Molecules Loaded per PLGA-*b*-PEG NP Prepared Using Emulsion-Diffusion Evaporation (EDE)

entry	PLGA-*b*-PEG NPs	mean size (nM)[a]	polydispersity index (PDI)[a]	encapsulation efficiency (%)[a] 4-OHT/ anti-miR-21	4-OHT/anti-miR-21 loading %	anti-miR molecules/NP
1	control NPs	108.7 ± 9.3	0.125			
2	4-OHT	110.7 ± 11.6	0.131	89.5 ± 4.8/−	4.8/−	
3	anti-miR-21	118.9 ± 8.4	0.128	−/23.7 ± 10.6	−/0.16	161 ± 67
4	4-OHT and anti-miR-21	134.5 ± 16.1	0.187	85 ± 6.2/20.6 ± 9.7	4.4/0.14	201 ± 93

[a]Average of three independent experiments.

Table 3. Size, Anti-miR-21 and 4-OHT Loading Percentage, and Number of Anti-miR-21 Molecules Loaded per PLGA-*b*-PEG NP Using the Water-in-Oil-in-Water (w/o/w) Method

entry	PLGA-*b*-PEG NPs	mean size (nM)[a]	polydispersity index (PDI)[a]	encapsulation efficiency (%)[a] 4-OHT/ anti-miR-21	4-OHT/anti-miR-21 loading %	anti-miR-21 molecules/NP
1	control NPs	132.5 ± 22.6	0.154			
2	4-OHT	134.6 ± 18.4	0.191	78.4 ± 5.6	3.92	
3	anti-miR-21	146.7 ± 16.3	0.162	58.2 ± 9.6	0.40	743 ± 122
4	4-OHT and anti-miR-21	167.8 ± 20.5	0.184	69.5 ± 8.1/51.5 ± 10.4	3.47/0.36	980 ± 197

[a]Average of three independent experiments.

Table 4. NPs Mean Sizes and Polydispersity Index (PDI) of PLGA-*b*-PEG NPs before and after Lyophilization Using Sucrose as a Lyoprotectant

entry	lyophilization of NPs	size[a] (nm) by EDE	PDI[a] by EDE	size[a] (nm) by w/o/w method	PDI[a] by w/o/w method
1	before lyophilization	115.7 ± 2.15	0.125 ± 0.009	138.8 ± 0.9	0.151 ± 0.01
2	after lyophilization without sucrose	120.1 ± 1.75	0.136 ± 0.008	143.8 ± 1.8	0.160 ± 0.03
3	after lyophilization with 10% sucrose	117.4 ± 2.20	0.100 ± 0.008	139.6 ± 1.5	0.145 ± 0.02
4	after lyophilization with 100% sucrose	117.8 ± 1.35	0.116 ± 0.007	140.7 ± 1.2	0.147 ± 0.03
5	after lyophilization with 1000% sucrose	130.4 ± 1.55	0.143 ± 0.025	150.8 ±. 2.5	0.171 ± 0.04

[a]Average of three DLS measurements.

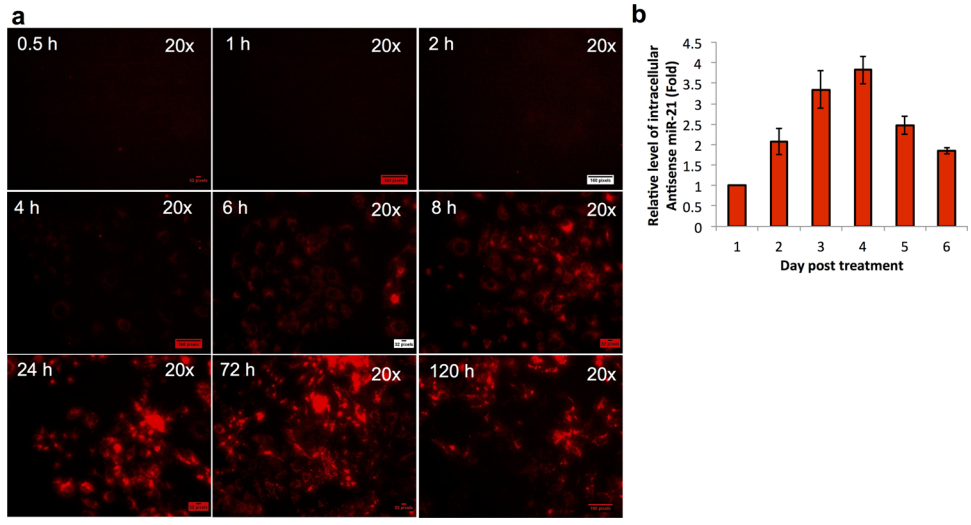

Figure 2. Time-dependent cellular uptake of 4-OHT and anti-miR-21 co-loaded PLGA NPs in MCF7 cells. (a) Microscopic images of Cy5 fluorescence from co-loaded Cy5−anti-miR-21 NPs. (b) Quantitative RT-PCR analysis of anti-miR-21 delivered by PLGA NPs in MCF7 cells over 6 days.

The PLGA-*b*-PEG NPs formulation for loading 4-OHT was optimized using the EDE method (Table 1), which is an efficient method for encapsulation of lipophilic drugs. Emulsification of PLGA-*b*-PEG and 4-OHT in ethyl acetate and 2% PVA aqueous solution at different sonication times (1−15 min) at 60% amplitude energy indicated that increasing the sonication time slightly decreased the size of the NPs (Table 1, entries 1−4). Replacing the ethyl acetate solvent with dichloromethane or DMF did not result a substantial difference in the size of the NPs (Table 1, entries 5 and 6).

After optimization of the 4-OHT-loaded PLGA-*b*-PEG NPs formed using the EDE method, several NPs were prepared under conditions shown in entry 1 of Table 1 for co-loading both 4-OHT and anti-miR-21. Calculations were performed on their size, zeta potential, and 4-OHT and anti-miR-21 loading percentage (Table 2). PLGA-*b*-PEG NPs formed in this way

DOI: 10.1021/mp500852s
Mol. Pharmaceutics 2015, 12, 2080−2092

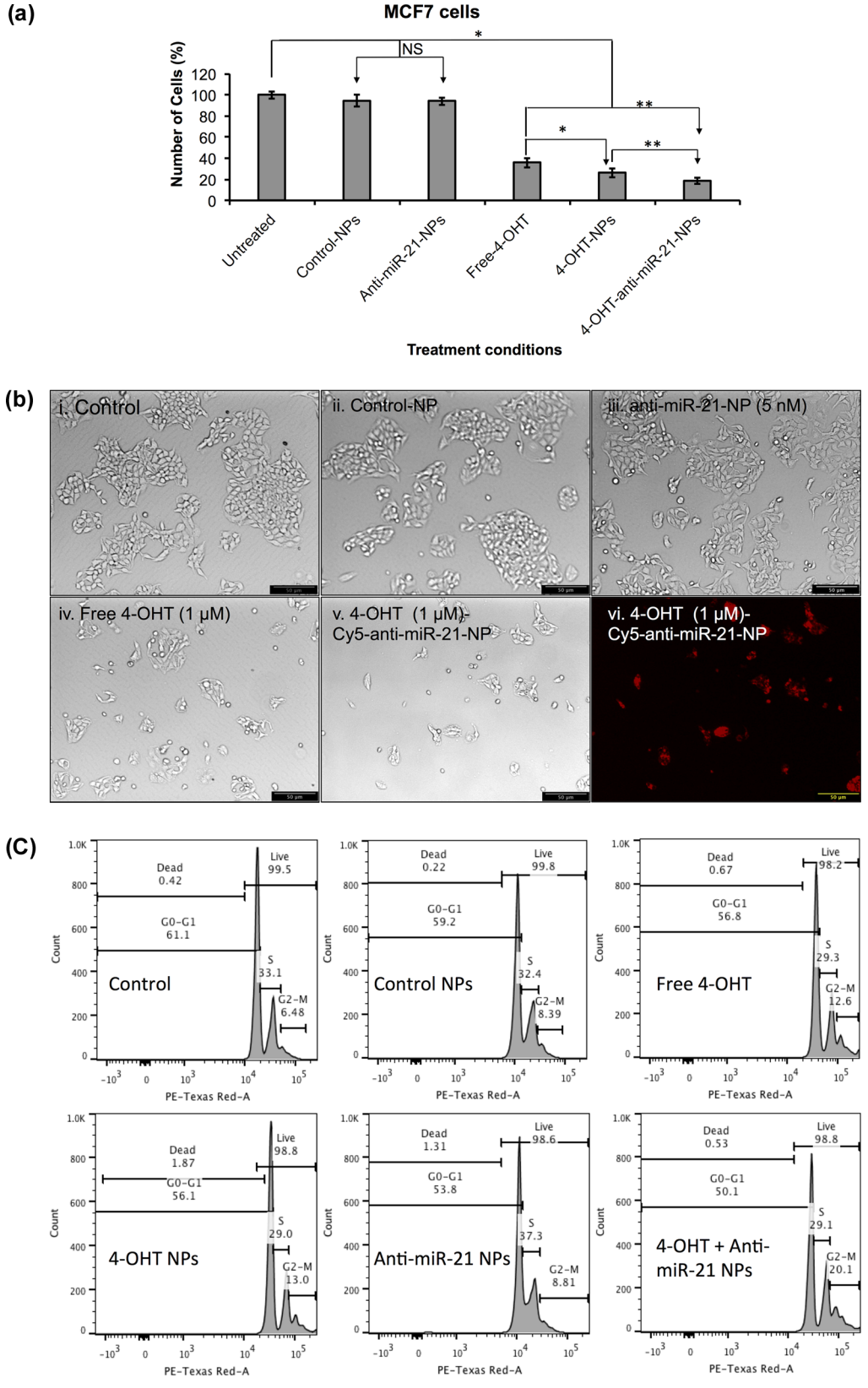

Figure 3. (a) Antiproliferation effect of 4-OHT and anti-miR-21-loaded NPs in MCF7 cells (* $p < 0.05$, ** $p < 0.01$, NS = not significant). (b) (i–v) Cell density by bright-field imaging: (i) control, (ii) treated with control NPs, (iii) treated with anti-miR-21 NPs, (iv) treated with free 4-OHT, and (v) treated with 4-OHT-Cy5-anti-miR-21 co-loaded NPs. (vi) Cy5 fluorescent signal from MCF7 cells treated with 4-OHT-Cy5-anti-miR-21 co-loaded NPs. (c) Flow cytometry analysis of MCF7 cells treated with free 4-OHT and anti-miR-21 NPs for 5 days.

were 108–134 nm in size and had 0.125–0.184 polydispersity index (PDI) values, which are optimal sizes and PDI values for PLGA-based drug delivery approaches to tumors[9] (Table 2, entries 1–4). The 4-OHT-loaded NPs provided 89.5%

DOI: 10.1021/mp500852s
Mol. Pharmaceutics 2015, 12, 2080–2092

Table 5. Cell Cycle Analysis by FACS

treatment conditions	dead cells	live cells	G0/G1	S	G2/M
control cells	0.42	99.5	61.1	33.1	6.48
control NPs	0.22	99.8	59.2	32.4	8.39
free 4-OHT	0.67	98.2	56.8	29.3	12.6
4-OHT NPs	1.87	98.8	56.1	29.0	13.0
anti-miR-21 NPs	1.31	98.6	53.8	37.3	8.81
4-OHT + anti-miR-21 NPs	0.53	98.8	50.1	29.1	20.1

encapsulation efficiency (ee), with 4.8% drug loading capacity (Table 2, entry 2). However, this method was able to achieve only a 23 ± 10% loading efficiency for anti-miR-21, which is possibly due to the hydrophilicity of anti-miR-21 (Table 2, entry 3). Co-loading of 4-OHT and anti-miR-21 also showed similar results as those for individually loaded NPs (Table 2, entry 4). The results of this experimentation led to the conclusion that the EDE method was very efficient for 4-OHT loading; however, the EDE method was not appropriate for loading anti-mIR-21 or co-encapsulating both 4-OHT and anti-miR-21.

In light of the low encapsulation efficiency (ee) of anti-miR-21 with the EDE method, subsequently, the water-in-oil-in-water (w/o/w) method was used to encapsulate PLGA-*b*-PEG NPs with anti-miR-21 and 4-OHT (Table 3). This is an efficient method for hydrophilic as well as hydrophobic drug encapsulation. The sizes of NPs prepared in this method were found to be in the range of 130−170 nm with PDI values of 0.154−0.191 (Table 3). 4-OHT and anti-miR-21 individually loaded in NPs prepared by this method afforded 78 and 58% ee, respectively (Table 3, entries 2 and 3). Co-encapsulation of both 4-OHT and anti-miR-21 delivered 69.5 and 51.5% ee, respectively (Table 3, entry 4).

To prevent slow hydrolysis of PLGA-*b*-PEG and to enable release of the entrapped drugs in solution,[47] sucrose was used as a lyoprotectant for long-time storage of NPs in freeze-dried powder form.[48] Subsequent optimization indicated that 10% sucrose was ideal for lyophilization of NPs (Table 4, entry 3). With the exception of 1000% sucrose use, in which few large sucrose particles were observed (Table 4, entry 5), these NPs did not display significant differences in PDI values before and after lyophilization (Table 4). The NPs, which were prepared by the double emulsion method, were used for all *in vitro* cell culture experiments.

Cell Uptake Studies by 4-OHT and Anti-miR-21 Co-loaded NPs in MCF7 Cells. To test the cellular uptake and internalization of NPs in cells, NPs prepared with a 10% substitution of Cy5 fluorescent dye-conjugated anti-miR-21 were used. The cell uptake studies were performed using Cy5−anti-miR-21 (10%, 0.5 nM), anti-miR-21 (90%, 4.5 nM), and 4-OHT (1 μM) co-loaded NPs in MCF7 cells and monitored by

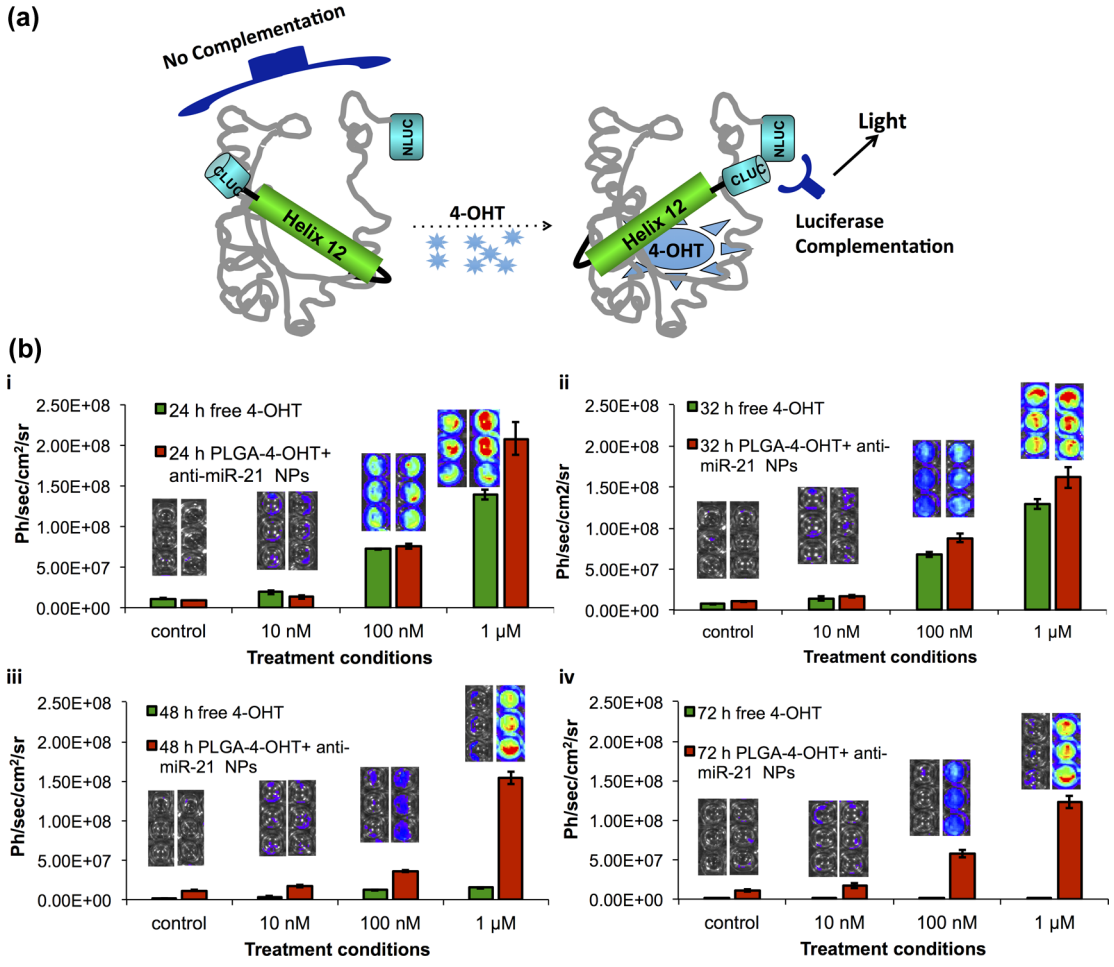

Figure 4. (a) Schematic illustration of NFluc−ER-LBD−CFluc fusion protein luciferase complementation activated by 4-OHT. (b) (i−iv) 4-OHT stability analysis in SkBr3−NFluc−ER-LBD−CFluc cells: (i) 4-OHT-ER Fluc-activation level after 24 h, (ii) 4-OHT-ER Fluc-activation level after 32 h, (iii) 4-OHT-ER Fluc-activation level after 48 h, and (iv) 4-OHT-ER Fluc-activation level after 72 h.

DOI: 10.1021/mp500852s
Mol. Pharmaceutics 2015, 12, 2080−2092

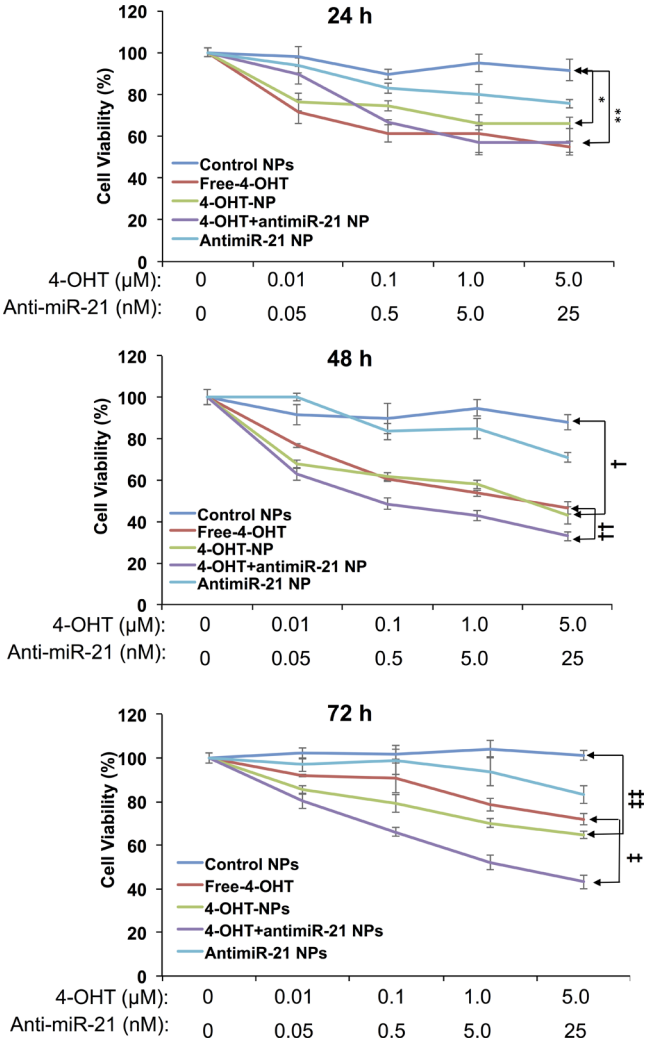

Figure 5. Dose response in MCF7 cells treated with free 4-OHT, 4-OHT-loaded NPs, anti-miR-21-loaded NPs, and 4-OHT−anti-miR-21 co-loaded NPs by MTT assay (24 h, * $p < 0.05$ control NPs vs 4-OHT NPs at 1 and 5 μM, ** $p < 0.01$ μM control NPs vs 4-OHT + anti-miR-21 NPs at 1 and 5 μM; 48 h, † $p < 0.01$ control NPs vs 4-OHT NPs at 1 and 5 μM; †† $p < 0.05$ free 4-OHT vs 4-OHT + anti-miR-21 NPs at 1 and 5 μM; 72 h, ‡ $p < 0.01$ free 4-OHT ss 4-OHT + anti-miR-21 NPs at 1 and 5 μM, ‡‡ $p < 0.01$ control NPs vs 4-OHT NPs at 1 μM and 5 μM).

fluorescent microscopy over time. The results suggested that the NPs' uptake was observed as early as 2 h after treatment and it continued to increase at 4, 6, and 8 h, with a large percentage of transfected cells at 24 h. After 24 h, the sustained release of Cy5−anti-miR-21 was observed at 48 and 72 h with slight increase in the Cy5 fluorescent signal. The Cy5 fluorescent signal started declining at 120 h post-treatment (Figure 2a).

Anti-miR-21 Intracellular Stability Analysis in MCF7 Cells. Microscopic imaging for the Cy5 signal can provide information regarding the intracellular delivery of NPs without providing much insight on the intracellular release and integrity of the delivered anti-miR-21. Hence, we tested the integrity of anti-miR-21 released from NPs delivered in cells by qRT-PCR. We used a custom-designed TaqMan probe for real-time qRT-PCR analysis. MCF7 cells were treated with anti-miR-21 and 4-OHT co-loaded NPs and quantified for the relative level of intracellular anti-miR-21 at different times post-treatment by qRT-PCR. The result indicated that the anti-miR-21 level gradually increased to 4-fold from days 1−4 and found a more than 2-fold increase even 6 days after initial delivery (Figure 2b). This result further signifies the slow and sustained release of anti-miR-21 by PLGA-*b*-PEG NPs delivered in cells.

Antiproliferative Effect of 4-OHT and Anti-miR-21 Co-loaded PLGA-*b*-PEG-NPs in ER Positive MCF7, ZR-75-1, BT-474, and 4T1 Breast Cancer Cells. Once it was confirmed that the delivery of NPs would result in the significant accumulation of anti-miR-21 in MCF7 cells, we proceeded to test the antiproliferative effect of the loaded 4-OHT on MCF7, ZR-75-1, BT-474, and 4T1 breast cancer cells. The proliferation of MCF7, ZR-75-1, BT-474, and 4T1 cells treated with 4-OHT and anti-miR-21 co-loaded PLGA-*b*-PEG NPs was studied and compared with cells treated with either free 4-OHT, control NPs, or anti-miR-21 loaded NPs. This data was also compared to the growth rate of respective untreated control cells (Figure 3a and Supporting Information Figure S1). The cells were treated with NPs loaded with 1 μM 4-OHT or 5 nM anti-miR-21 or co-loaded with both. The cells treated with 1 μM equivalent of control NPs were used as control. The cells were incubated at 37 °C with 5% CO_2 in a humidified chamber. After 24 h, cells were washed with PBS, fresh medium with 2% charcoal-treated FBS was added, cells were incubated further for 5 days, and cell proliferation was measured by counting the cells. All four cell lines showed a significant ($p < 0.05$) antiproliferative effect in response to the treatment with free 4-OHT, 4-OHT NPs, and NPs co-loaded with 4-OHT and anti-miR-21. The results indicated that 4-OHT and anti-miR-21 co-loaded NPs significantly inhibited the proliferation of MCF7 (5.4-fold, $p < 0.01$), ZR-75-1 (1.5-fold, $p < 0.01$), BT-474 (2.4-fold, $p < 0.01$), and 4T1 (2.2-fold, $p < 0.01$) cells compared to untreated cells. Similarly, 4-OHT individually loaded NPs considerably inhibited the proliferation of MCF7 (3.9-fold, $p < 0.01$), ZR-75-1 (1.4-fold, $p < 0.01$), BT-474 (1.7-fold, $p < 0.01$), and 4T1 (1.8-fold, $p < 0.01$) cells compared to untreated cells. Moreover, free 4-OHT also inhibited the proliferation of MCF7 (2.8-fold, $p < 0.01$), ZR-75-1 (1.2-fold, $p < 0.01$), BT-474 (1.6-fold, $p < 0.01$), and 4T1 (1.4-fold, $p < 0.01$) cells. Remarkably, 4-OHT and anti-miR-21 co-loaded NPs showed significantly higher antiproliferative effects compare to those of free-4-OHT in MCF7 (1.94-fold, $p < 0.05$), ZR-75-1 (1.5-fold, $p < 0.05$), BT-474 (1.5-fold, $p < 0.05$), and 4T1 (1.6-fold, $p < 0.05$) cells and showed moderately higher antiproliferative effects compared to those of 4-OHT NPs in MCF7 (1.4-fold, $p < 0.05$), ZR-75-1 (1.1-fold, $p < 0.05$), BT-474 (1.4-fold, $p < 0.05$), and 4T1 (1.2-fold, $p < 0.05$) cells (Figure 3a and Supporting Information Figure S1). Furthermore, 4-OHT individually loaded NPs showed moderately higher antiproliferative effects compared to those of free-4-OHT in all four cell lines [MCF7 cells (1.5-fold, $p < 0.05$), ZR-75-1 cells (1.4-fold, $p < 0.05$), BT-474 cells (1.1-fold, $p < 0.05$), and 4T1 cells (1.3-fold, $p < 0.05$)]. It is noteworthy that anti-miR-21-loaded NPs and control NPs did not show any antiproliferative effects in all four cells lines, signifying that anti-miR-21 was not cytotoxic at the 5 nM concentration used for the study (Figure 3a and Supporting Information Figure S1). The higher antiproliferative effect of 4-OHT-loaded NPs compared to that of free 4-OHT observed in this study is due to the slow release property PLGA NPs, which maintains the availability of stable active 4-OHT, resulting in a prolonged functional effect. Free 4-OHT undergoes degradation overtime, whereas NPs release the active 4-OHT in a slow and sustained manner. In addition, we washed cells 24 h after treatment so that no NPs were left in the medium for further endocytosis or free 4-OHT for further cell uptake; hence, 4-OHT

DOI: 10.1021/mp500852s
Mol. Pharmaceutics 2015, 12, 2080−2092

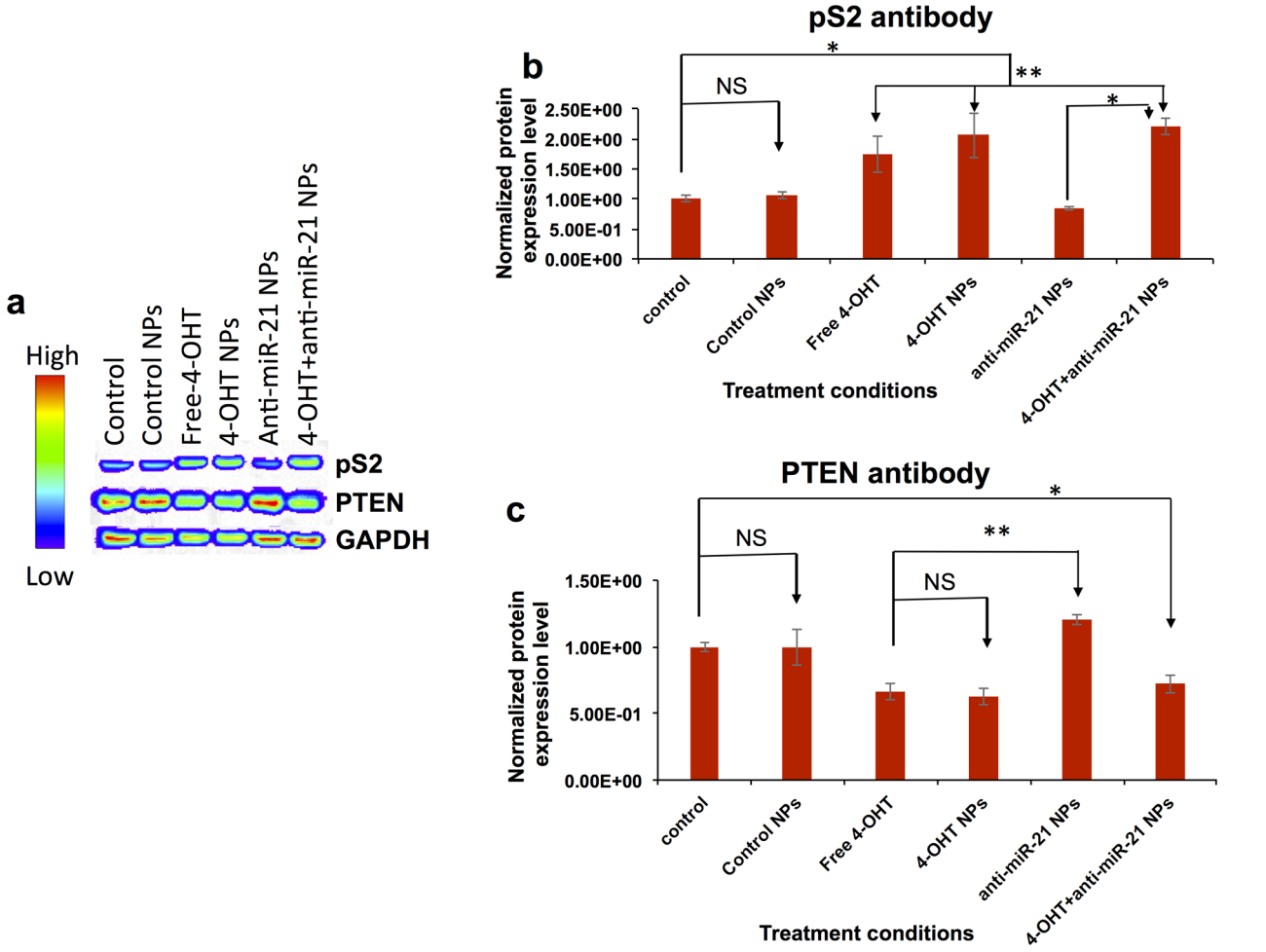

Figure 6. Western blot analysis of MCF7 cells treated with free 4-OHT and 4-OHT with and without anti-miR-21 co-loaded NPs for 5 days. (a) Pseudocolor images of pS2, PTEN, and GAPDH proteins stained with respective antibodies and imaged by optical CCD camera. (b, c) Absolute quantification of photon signals from panel (a) for pS2 (* $p < 0.01$, ** $p < 0.05$) (b) and PTEN (* $p < 0.01$, ** $p < 0.05$) (c) proteins expression levels.

loaded in NPs displayed higher antiproliferative effects. The cells treated with NPs loaded with 4-OHT and co-loaded with 4-OHT and anti-miR-21 experience an equal effect in the beginning due to the initial burst release of 4-OHT, which is similar for both NPs. The increased therapeutic effect that we observed in cells treated with NPs co-loaded with 4-OHT and anti-miR-21 over time (1.4-fold) was achieved through the cumulative actions of both anti-miR-21 and 4-OHT. The observed value of a 1.9-fold higher effect by co-loaded NPs compared to that in cells treated with free 4-OHT confirms this point. Moreover, anti-miR-21 functions as an endogenous regulator of gene expression, which sensitizes cells and improves their response to chemotherapy. Since anti-miR-21 is not expected to produce any independent antiproliferative effect that contributes to a cumulative effect, it does improve the effect of 4-OHT.

In addition, the phase-contrast microscopic images of MCF7 cells treated with different NPs show a clear reduction in the density of cells treated with either free 4-OHT or the 4-OHT–anti-miR-21 co-loaded NPs (Figure 3b). Since 10% of anti-miR-21 was substituted with Cy5–anti-miR-21, the significant accumulation of co-loaded NPs was observed inside the cells even 5 days after initial treatment by fluorescent imaging (Figure 3b-vi). Flow cytometry analysis of the above treated samples indicated that no significant percentage of apoptotic cells was present in MCF7 samples. This verified that the treatment of cells with NPs co-loaded with 4-OHT and anti-miR-21 was not cytotoxic at the concentrations used (Figure 3c). Cell cycle status by flow cytometry analysis showed no significant difference between untreated cells and cells treated with control NPs. In contrast, cells treated with 4-OHT–anti-miR-21 co-loaded NPs showed a significant reduction in G0/G1 phase, a significant increase in G2/M phase, and a decrease in S phase, which indicated cell growth arrest. Free 4-OHT and 4-OHT-loaded NPs also showed a reduction in G0/G1, S, and G2/M phases. Surprisingly, anti-miR-21-loaded NPs showed an increase in S phase and a decrease in G0/G1 phase, but not G2/M phase. This suggests that anti-miR-21 might be playing a crucial role in the higher cell growth arrest observed when it is coadministered with 4-OHT in comparison to that from free 4-OHT and 4-OHT NPs (Figure 3c and Table 5).

4-OHT Intracellular Stability Analysis by Reporter Protein Complementation Assay in SkBr3 Cells Stably Expressing NFluc–ER-LBD–CFluc Sensor Fusion Protein. The stability of encapsulated 4-OHT was evaluated by its biological activity in order to confirm that the delivery system developed in this study was effectively increasing the bioavailability 4-OHT by reducing its rapid degradation in the medium. We used a reporter protein complementation system, which we developed previously,[49] where the conformational switch induced by the binding of estrogen and its analogues to

DOI: 10.1021/mp500852s
Mol. Pharmaceutics 2015, 12, 2080–2092

ERs can be indirectly measured through the complementation of firefly luciferase fragments fused at the NH_2 and COOH terminal of ER-ligand binding domain (Figure 4a). To measure the intracellular stability of 4-OHT in this study, we treated SkBr3 cells stably expressing the complementation sensor with different concentrations of either free 4-OHT or NPs co-loaded with 4-OHT and anti-miR-21. Firefly luciferase (Fluc) signal was then measured at different time points post-treatment by bioluminescence imaging. Fluc signal was normalized to the number of cells, measured using parallel MTT assays. A moderately higher bioluminescence signal was obtained from cells treated with co-loaded NPs compared to that from cells treated with free 4-OHT at 24 and 32 h post-treatment, confirming higher stability in cells (Figure 4b-i,ii). Differences were more pronounced at later time points; encapsulated 4-OHT showed significantly higher stability than that from cells treated with free 4-OHT at 48 h ($p < 0.01$ at 10 nM, 100 nM, and 1 μM, respectively) and 72 h ($p < 0.01$ at 10 nM, 100 nM, and 1 μM, respectively) (Figure 4b-iii,iv). At the highest concentration administered (1 μM), the stability of NPs loaded with 4-OHT at 72 h was ~222 ± 50-fold higher than that of free 4-OHT. We conclude that the stability of 4-OHT was increased by PLGA-*b*-PEG NP encapsulation due to its slow and sustained release capability, whereas free 4-OHT degraded rapidly in the cells. These results demonstrate that the encapsulation of 4-OHT in PLGA-*b*-PEG NPs not only improves the delivery of 4-OHT but also increases its stability inside the cells.

Dose-Dependent Effect of 4-OHT and Anti-miR-21 Co-loaded PLGA-PEG NPs on MCF7 Cell Proliferation. Since 4-OHT is an active metabolite of TAM, which functions as a cytostatic drug, and anti-miR-21 silences the endogenous miR-21, we investigated the effect of 4-OHT and anti-miR-21 cotreatment on MCF7 cell proliferation. Dose study analysis of free 4-OHT and 4-OHT and anti-miR-21 loaded PLGA-*b*-PEG NPs was evaluated in MCF7 cells using MTT assays at 24, 48, and 72 h post-treatment (Figure 5). Treatment with control NPs or anti-miR-21 NPs did not have any considerable antiproliferative effects. In contrast, treatment with free 4-OHT, 4-OHT NPs, or 4-OHT−anti-miR-21 co-loaded NPs resulted in a dose-dependent reduction in cell proliferation, and the highest antiproliferative effect was achieved with the co-loaded NPs. There was a significant reduction in the viability of cells treated with 4-OHT−anti-miR-21 co-loaded NPs compared to that of untreated cells ($p < 0.01$) and those treated with control NPs ($p < 0.01$ at 1 and 5 μM). While free 4-OHT appeared to perform as well as encapsulated 4-OHT at 24 h post-treatment, 4-OHT−anti-miR-21 co-loaded NPs showed significantly higher antiproliferative effects at 48 h ($p < 0.05$, compared to free 4-OHT at 1 and 5 μM) and 72 h ($p < 0.01$, compared to free 4-OHT at 1 and 5 μM) post-treatment (Figure 5).

Immunoblot Analysis To Evaluate the Downstream Effect of 4-OHT and Anti-miR-21 Co-loaded PLGA-PEG NPs in MCF7 and ZR-75-1 Cell Lines. To further confirm the antiproliferative effect induced by 4-OHT and anti-miR-21 co-loaded NPs in breast cancer cells, we evaluated the protein expression levels of the downstream targets of ER and miR-21, such as pS2 and phosphatase and tensin homologue (PTEN), respectively (Figure 6 and Supporting Information Figure S2). As anticipated, an increase in pS2 protein expression was observed in MCF7 and ZR-75-1 cells treated with free 4-OHT, 4-OHT-loaded NPs, and co-loaded NPs ($p < 0.01$) compared to untreated cells (Figure 6a,b and Supporting Information Figure S2a,b). An increase in miR-21 target protein PTEN expression was observed only in cells treated with anti-miR-21-loaded NPs ($p < 0.01$, untreated cells vs anti-miR-21 treated cells) (Figure 6a,c and Supporting Information Figure S2a,c). However, very low expression levels of pS2 and PTEN were observed in ZR-75-1 cells compared to those in MCF7 cells. The cells treated with free 4-OHT and 4-OHT NPs showed significant downregulation of PTEN. In contrast, cells treated with 4-OHT−anti-miR-21 co-loaded NPs showed a significant increase in PTEN protein expression (Figure 6a,c). These results clearly confirm that cotreatment of anti-miR-21 can upregulates PTEN even in the presence of 4-OHT. In this study, the immunoblot analysis was performed 5 days after respective treatment conditions. The low PTEN level in cells treated with anti-miR-21-loaded NPs observed in this study could possibly be due to a suboptimal post-treatment time point used for immunoblot analysis. Since we delivered only 5 nM anti-miR-21 to target endogenous miR-21 nearly 5 days before the immunoblot analysis, there was not enough anti-miR-21 available at the time selected for the study to further block endogenous miR-21 to enhance PTEN expression.

■ CONCLUSIONS

In summary, we have successfully developed efficient methods for encapsulation of 4-OHT in PLGA-*b*-PEG NPs by using the EDE method and for coencapsulation of 4-OHT and anti-miR-21 by using the w/o/w method. 4-OHT and anti-miR-21 co-loaded NPs demonstrated significant antiproliferative effects in MCF7 cells and moderate antiproliferative effects in ZR-75-1, BT-474, and 4T1 ER+ breast cancer cells. Co-delivery of 4-OHT and anti-miR-21 had an additive effect in reducing ER+ breast cancer cell proliferation without any significant cytotoxicity. Encapsulation of 4-OHT also increased the stability of this drug, measured using a reporter protein complementation assay. The improvement in 4-OHT stability was ~222 ± 50-fold more when encapsulated in PLGA-*b*-PEG-NP compared to that of free 4-OHT at 1 μM treatment concentrations. The results of this study demonstrate that PLGA-*b*-PEG NPs are effective nanocarriers that can be used for the co-delivery of 4-OHT and anti-miR-21 to cancer cells. We also demonstrated the therapeutic potential of 4-OHT and anti-miR-21 co-delivery in inhibiting cancer cell proliferation.

■ ASSOCIATED CONTENT

Supporting Information

Figure S1: Antiproliferative effect of 4-OHT and anti-miR-21-loaded NPs on ZR-75-1, 4T1, and BT-474 breast cancer cells. Figure S2: Western blot analysis of ZR-75-1 cells treated with free 4-OHT and 4-OHT with and without anti-miR-21 co-loaded NPs for 5 days. This material is available free of charge via the Internet at http://pubs.acs.org.

■ AUTHOR INFORMATION

Corresponding Author

*Phone: +1-650-725-6097. E-mail: paulmur8@stanford.edu.

Notes

The authors declare no competing financial interest.

■ ACKNOWLEDGMENTS

This work was partially supported by the National Institutes of Health (NIH grant R01CA161091 to R.P.). The authors thank Dr. Sanjiv Sam Gambhir, Chairman, Department of Radiology, Stanford University, for his constant support and the Canary Center at Stanford for facilities and support. The authors would

DOI: 10.1021/mp500852s
Mol. Pharmaceutics 2015, 12, 2080−2092

like to thank Dr. Anjali Sheahan, Stanford University, and Dr. Dave Seapy, Texas A&M University at Qatar, for their time in proof reading the manuscript.

REFERENCES

(1) Kamangar, F.; Dores, G. M.; Anderson, W. F. Patterns of cancer incidence, mortality, and prevalence across five continents: defining priorities to reduce cancer disparities in different geographic regions of the world. *J. Clin. Oncol.* **2006**, *24*, 2137−50.

(2) Rozhkova, E. A.; Zhi, F.; Dong, H.; Jia, X.; Guo, W.; Lu, H.; Yang, Y.; Ju, H.; Zhang, X.; Hu, Y. Functionalized graphene oxide mediated adriamycin delivery and miR-21 gene silencing to overcome tumor multidrug resistance in vitro. *PLoS One* **2013**, *8*, e60034.

(3) Soma, C. E.; Dubernet, C.; Bentolila, D.; Benita, S.; Couvreur, P. Reversion of multidrug resistance by co-encapsulation of doxorubicin and cyclosporin A in polyalkylcyanoacrylate nanoparticles. *Biomaterials* **2000**, *21*, 1−7.

(4) Greco, F.; Vicent, M. J. Combination therapy: opportunities and challenges for polymer−drug conjugates as anticancer nanomedicines. *Adv. Drug Delivery Rev.* **2009**, *61*, 1203−13.

(5) Sun, T. M.; Du, J. Z.; Yao, Y. D.; Mao, C. Q.; Dou, S.; Huang, S. Y.; Zhang, P. Z.; Leong, K. W.; Song, E. W.; Wang, J. Simultaneous delivery of siRNA and paclitaxel via a "two-in-one" micelleplex promotes synergistic tumor suppression. *ACS Nano* **2011**, *5*, 1483−94.

(6) Xiong, X. B.; Lavasanifar, A. Traceable multifunctional micellar nanocarriers for cancer-targeted co-delivery of MDR-1 siRNA and doxorubicin. *ACS Nano* **2011**, *5*, 5202−13.

(7) Tan, B.; Piwnica-Worms, D.; Ratner, L. Multidrug resistance transporters and modulation. *Curr. Opin. Oncol.* **2000**, *12*, 450−8.

(8) Lee, C. H. Reversing agents for ATP-binding cassette drug transporters. *Methods Mol. Biol.* **2010**, *596*, 325−40.

(9) Devulapally, R.; Paulmurugan, R. Polymer nanoparticles for drug and small silencing RNA delivery to treat cancers of different phenotypes. *Wiley Interdiscip. Rev.: Nanomed. Nanobiotechnol.* **2014**, *6*, 40−60.

(10) Desta, Z.; Ward, B. A.; Soukhova, N. V.; Flockhart, D. A. Comprehensive evaluation of tamoxifen sequential biotransformation by the human cytochrome P450 system in vitro: prominent roles for CYP3A and CYP2D6. *J. Pharmacol. Exp. Ther.* **2004**, *310*, 1062−75.

(11) Hoskins, J. M.; Carey, L. A.; McLeod, H. L. CYP2D6 and tamoxifen: DNA matters in breast cancer. *Nat. Rev. Cancer* **2009**, *9*, 576−86.

(12) Johnston, S. R. New strategies in estrogen receptor-positive breast cancer. *Clin. Cancer Res.* **2010**, *16*, 1979−87.

(13) Koshida, S.; Narita, T.; Kato, H.; Yoshida, S.; Taga, T.; Ohta, S.; Takeuchi, Y. Estrogen receptor expression and estrogen receptor-independent cytotoxic effects of tamoxifen on malignant rhabdoid tumor cells in vitro. *Jpn. J. Cancer Res.* **2002**, *93*, 1351−7.

(14) Coezy, E.; Borgna, J. L.; Rochefort, H. Tamoxifen and metabolites in MCF7 cells: correlation between binding to estrogen receptor and inhibition of cell growth. *Cancer Res.* **1982**, *42*, 317−23.

(15) Vignon, F.; Bouton, M. M.; Rochefort, H. Antiestrogens inhibit the mitogenic effect of growth factors on breast cancer cells in the total absence of estrogens. *Biochem. Biophys. Res. Commun.* **1987**, *146*, 1502−8.

(16) Reddel, R. R.; Murphy, L. C.; Sutherland, R. L. Effects of biologically active metabolites of tamoxifen on the proliferation kinetics of MCF-7 human breast cancer cells in vitro. *Cancer Res.* **1983**, *43*, 4618−24.

(17) Malet, C.; Gompel, A.; Spritzer, P.; Bricout, N.; Yaneva, H.; Mowszowicz, I.; Kuttenn, F.; Mauvais-Jarvis, P. Tamoxifen and hydroxytamoxifen isomers versus estradiol effects on normal human breast cells in culture. *Cancer Res.* **1988**, *48*, 7193−9.

(18) Murphy, C. S.; Langan-Fahey, S. M.; McCague, R.; Jordan, V. C. Structure−function relationships of hydroxylated metabolites of tamoxifen that control the proliferation of estrogen-responsive T47D breast cancer cells in vitro. *Mol. Pharmacol.* **1990**, *38*, 737−43.

(19) Furr, B. J.; Jordan, V. C. The pharmacology and clinical uses of tamoxifen. *Pharmacol. Ther.* **1984**, *25*, 127−205.

(20) Fisher, B.; Costantino, J. P.; Wickerham, D. L.; Redmond, C. K.; Kavanah, M.; Cronin, W. M.; Vogel, V.; Robidoux, A.; Dimitrov, N.; Atkins, J.; Daly, M.; Wieand, S.; Tan-Chiu, E.; Ford, L.; Wolmark, N. Tamoxifen for prevention of breast cancer: report of the National Surgical Adjuvant Breast and Bowel Project P-1 Study. *J. Natl. Cancer Inst.* **1998**, *90*, 1371−88.

(21) Taylor, C. M.; Blanchard, B.; Zava, D. T. Estrogen receptor-mediated and cytotoxic effects of the antiestrogens tamoxifen and 4-hydroxytamoxifen. *Cancer Res.* **1984**, *44*, 1409−14.

(22) Fisher, B.; Dignam, J.; Wolmark, N.; Wickerham, D. L.; Fisher, E. R.; Mamounas, E.; Smith, R.; Begovic, M.; Dimitrov, N. V.; Margolese, R. G.; Kardinal, C. G.; Kavanah, M. T.; Fehrenbacher, L.; Oishi, R. H. Tamoxifen in treatment of intraductal breast cancer: National Surgical Adjuvant Breast and Bowel Project B-24 randomised controlled trial. *Lancet* **1999**, *353*, 1993−2000.

(23) Rouanet, P.; Linares-Cruz, G.; Dravet, F.; Poujol, S.; Gourgou, S.; Simony-Lafontaine, J.; Grenier, J.; Kramar, A.; Girault, J.; Le Nestour, E.; Maudelonde, T. Neoadjuvant percutaneous 4-hydroxytamoxifen decreases breast tumoral cell proliferation: a prospective controlled randomized study comparing three doses of 4-hydroxytamoxifen gel to oral tamoxifen. *J. Clin. Oncol.* **2005**, *23*, 2980−7.

(24) Mauvais-Javis, P.; Baudot, N.; Castaigne, D.; Banzet, P.; Kuttenn, F. trans-4-Hydroxytamoxifen concentration and metabolism after local percutaneous administration to human breast. *Cancer Res.* **1986**, *46*, 1521−5.

(25) Si, M. L.; Zhu, S.; Wu, H.; Lu, Z.; Wu, F.; Mo, Y. Y. miR-21-mediated tumor growth. *Oncogene* **2007**, *26*, 2799−803.

(26) Yan, L. X.; Huang, X. F.; Shao, Q.; Huang, M. Y.; Deng, L.; Wu, Q. L.; Zeng, Y. X.; Shao, J. Y. MicroRNA miR-21 overexpression in human breast cancer is associated with advanced clinical stage, lymph node metastasis and patient poor prognosis. *RNA* **2008**, *14*, 2348−60.

(27) Yan, L. X.; Wu, Q. N.; Zhang, Y.; Li, Y. Y.; Liao, D. Z.; Hou, J. H.; Fu, J.; Zeng, M. S.; Yun, J. P.; Wu, Q. L.; Zeng, Y. X.; Shao, J. Y. Knockdown of miR-21 in human breast cancer cell lines inhibits proliferation, in vitro migration and in vivo tumor growth. *Breast Cancer Res.* **2011**, *13*, R2.

(28) Devulapally, R.; Sekar, T. V.; Paulmurugan, R. Anti-proliferative effect of 4-hydroxytamoxifen loaded PLGA-b-PEG nanoparticles in human breast cancer cell lines expressing different levels of Her2 receptor. *World Mol. Imaging Congr.* **2013**, 476.

(29) Pecot, C. V.; Calin, G. A.; Coleman, R. L.; Lopez-Berestein, G.; Sood, A. K. RNA interference in the clinic: challenges and future directions. *Nat. Rev. Cancer* **2011**, *11*, 59−67.

(30) Mitchell, P. S.; Parkin, R. K.; Kroh, E. M.; Fritz, B. R.; Wyman, S. K.; Pogosova-Agadjanyan, E. L.; Peterson, A.; Noteboom, J.; O'Briant, K. C.; Allen, A.; Lin, D. W.; Urban, N.; Drescher, C. W.; Knudsen, B. S.; Stirewalt, D. L.; Gentleman, R.; Vessella, R. L.; Nelson, P. S.; Martin, D. B.; Tewari, M. Circulating microRNAs as stable blood-based markers for cancer detection. *Proc. Natl. Acad. Sci. U.S.A.* **2008**, *105*, 10513−8.

(31) Trotta, F.; Dianzani, C.; Caldera, F.; Mognetti, B.; Cavalli, R. The application of nanosponges to cancer drug delivery. *Expert Opin. Drug Delivery* **2014**, *11*, 931−41.

(32) Urbinati, G.; Marsaud, V.; Renoir, J. M.; Sola, B. 4-Hydroxy-tamoxifen-loaded liposomes have potent anti-myeloma activity. *Leuk. Lymphoma* **2013**, *54*, 1808−10.

(33) Urbinati, G.; Audisio, D.; Marsaud, V.; Plassat, V.; Arpicco, S.; Sola, B.; Fattal, E.; Renoir, J.-M. Therapeutic potential of new 4-hydroxy-tamoxifen-loaded pH-gradient liposomes in a multiple myeloma experimental model. *Pharm. Res.* **2009**, *27*, 327−39.

(34) Agudelo, D.; Sanyakamdhorn, S.; Nafisi, S.; Tajmir-Riahi, H. A. Transporting antitumor drug tamoxifen and its metabolites, 4-hydroxytamoxifen and endoxifen by chitosan nanoparticles. *PLoS One* **2013**, *8*, e60250.

(35) Escobar Ivirico, J. L.; Beaumont, M.; Garcia Cruz, D. M.; Gomez-Pinedo, U. A.; Pradas, M. M. Cytotoxic effect of 4-hydroxytamoxifen conjugate material on human Schwann cells: Synthesis and characterization. *J. Bioact. Compat. Polym.* **2013**, *28*, 574−89.

DOI: 10.1021/mp500852s
Mol. Pharmaceutics 2015, 12, 2080−2092

(36) Chen, M.; Pierstorff, E. D.; Lam, R.; Li, S. Y.; Huang, H.; Osawa, E.; Ho, D. Nanodiamond-mediated delivery of water-insoluble therapeutics. *ACS Nano* **2009**, *3*, 2016−22.
(37) Ren, Y.; Kang, C. S.; Yuan, X. B.; Zhou, X.; Xu, P.; Han, L.; Wang, G. X.; Jia, Z.; Zhong, Y.; Yu, S.; Sheng, J.; Pu, P. Y. Co-delivery of as-miR-21 and 5-FU by poly(amidoamine) dendrimer attenuates human glioma cell growth in vitro. *J. Biomater. Sci., Polym. Ed.* **2010**, *21*, 303−14.
(38) Costa, P. M.; Cardoso, A. L.; Mendonça, L. S.; Serani, A.; Custódia, C.; Conceição, M.; Simões, S.; Moreira, J. N.; Pereira de Almeida, L.; Pedroso de Lima, M. C. Tumor-targeted chlorotoxin-coupled nanoparticles for nucleic acid delivery to glioblastoma cells: a promising system for glioblastoma treatment. *Mol. Ther.—Nucleic Acids* **2013**, *2*, e100.
(39) Danhier, F.; Ansorena, E.; Silva, J. M.; Coco, R.; Le Breton, A.; Preat, V. PLGA-based nanoparticles: an overview of biomedical applications. *J. Controlled Release* **2012**, *161*, 505−22.
(40) Locatelli, E.; Comes Franchini, M. Biodegradable PLGA-b-PEG polymeric nanoparticles: synthesis, properties, and nanomedical applications as drug delivery system. *J. Nanopart. Res.* **2012**, *14*, 1316.
(41) Devulapally, R.; Sekar, N. M.; Sekar, T. V.; Foygel, K.; Massoud, T. F.; Willmann, J. K.; Paulmurugan, R. Polymer nanoparticles mediated codelivery of antimiR-10b and antimiR-21 for achieving triple negative breast cancer therapy. *ACS Nano* **2015**, *9*, 2290−302.
(42) Wang, T. Y.; Choe, J. W.; Pu, K.; Devulapally, R.; Bachawal, S.; Machtaler, S.; Chowdhury, S. M.; Luong, R.; Tian, L.; Khuri-Yakub, B.; Rao, J.; Paulmurugan, R.; Willmann, J. K. Ultrasound-guided delivery of microRNA loaded nanoparticles into cancer. *J. Controlled Release* **2015**, *203C*, 99−108.
(43) Wang, T.-Y.; Choe, J. W.; Machtaler, S.; Devulapally, R.; Khuri-Yakub, P. T.; Paulmurugan, R.; Willmann, J. K. *Effects of ultrasound parameters on cavitation-assisted delivery of PLGA-PEG nanoparticles into tumors: phantom study and preliminary in vivo results*, Radiological Society of North America 2013 Scientific Assembly and Annual Meeting, Chicago, IL, December 1−6, 2013; SSA21-08.
(44) Wang, T. Y.; C, J. W.; Machtaler, S.; Devulapally, R.; Khuri-Yakub, B.; Paulmurugan, R.; Willmann, J. K. Optimizing acoustic cavitation for ultrasound-microbubble-mediated delivery of PLGA nanoparticles into tumors:phantom study and preliminary in vivo results. *World Mol. Imaging Congr.* **2013**, 259.
(45) Woodrow, K. A.; Cu, Y.; Booth, C. J.; Saucier-Sawyer, J. K.; Wood, M. J.; Saltzman, W. M. Intravaginal gene silencing using biodegradable polymer nanoparticles densely loaded with small-interfering RNA. *Nat. Mater.* **2009**, *8*, 526−33.
(46) Paulmurugan, R.; Sekar, N. M.; Sekar, T. V. Biodegradable polymer nanocarriers for therapeutic antisense microRNA delivery in living animals. *Proc. SPIE* **2012**, *8232*, 823208.
(47) Makadia, H. K.; Siegel, S. J. Poly lactic-co-glycolic acid (PLGA) as biodegradable controlled drug delivery carrier. *Polymers (Basel, Switz.)* **2011**, *3*, 1377−1397.
(48) Abdelwahed, W.; Degobert, G.; Stainmesse, S.; Fessi, H. Freeze-drying of nanoparticles: formulation, process and storage considerations. *Adv. Drug Delivery Rev.* **2006**, *58*, 1688−713.
(49) Paulmurugan, R.; Tamrazi, A.; Katzenellenbogen, J. A.; Katzenellenbogen, B. S.; Gambhir, S. S. A human estrogen receptor (ER)alpha mutation with differential responsiveness to nonsteroidal ligands: novel approaches for studying mechanism of ER action. *Mol. Endocrinol.* **2008**, *22*, 1552−64.

DOI: 10.1021/mp500852s
Mol. Pharmaceutics 2015, 12, 2080−2092